ISBN: 978-3-95450-231-8 ISSN: 2673-5490 doi: 10.18429/JACoW-IPAC2023-WEPL153

IMPEDANCE ANALYSIS OF DEFORMABLE RF CONTACT BRIDGES FOR HIGH LUMINOSITY LHC

P. Krkotić*, S. Calatroni†, M. Neroni, C. Völlinger, B. Salvant, V. Baglin, C. Garion, and G. Bregliozzi
CERN, 1211 Meyrin, Geneva, Switzerland

Abstract

In order to maintain the continuity of the vacuum system wall and comply with beam stability limits, radio frequency contact bridges are utilised as transitional elements in beam vacuum line interconnections. These radio frequency contact bridges must absorb and correct longitudinal, angular, and transverse misalignments brought on by mechanical motions during assembly, alignment, operating phases and thermal influences during accelerator operation. A deformable thin-walled copper beryllium structure is the foundation of a novel deformable radio frequency contact bridge concept that satisfies the above criteria without using conventional sliding contacts. To assess the feasibility of implementing such deformable radio frequency contact bridges in the High-Luminosity LHC, the longitudinal, dipolar, and quadrupolar components of the beam impedance in the two transverse planes were determined using electromagnetic simulations.

INTRODUCTION

Leak-tight bellows are frequently used to make up for mechanical displacements of adjacent vacuum chambers caused, for example, by thermal transients or during assembly and commissioning. However, these bellows have a high beam coupling impedance because of their geometric design and low-conductivity material. In order to maintain the continuity of the vacuum chamber while still achieving adequate beam stability, radio frequency (RF) contacts are employed as transitional elements in vacuum chamber interconnections in combination with bellows. The RF contacts carry the beam image current produced by the circulating particles assuring the electrical continuity between the adjacent vacuum chambers. This reduces the beam coupling impedance by electromagnetically shielding the outer bellows.

A new concept design of RF contacts was proposed in Ref. [1] for the High-Luminosity (HL)-LHC upgrade whose immediate improvement is that the RF contact no longer slides when the vacuum chamber moves longitudinally. Instead, the RF fingers themselves are deformable and fixed on the ends; in this way, permitting a continuous connection between adjacent vacuum chambers by stretching and compacting. The design of the deformable RF contacts (DRF) is based on thin-walled copper beryllium structure with three V-shaped convolutions as visible in Fig. 1. The convolutions include longitudinal cut-outs of 1.4 mm width that forms RF fingers of 3 mm width. This guarantees electrical continuity but could induce trapped modes with high beam impedance. The DRF contact bridges come in various sizes,

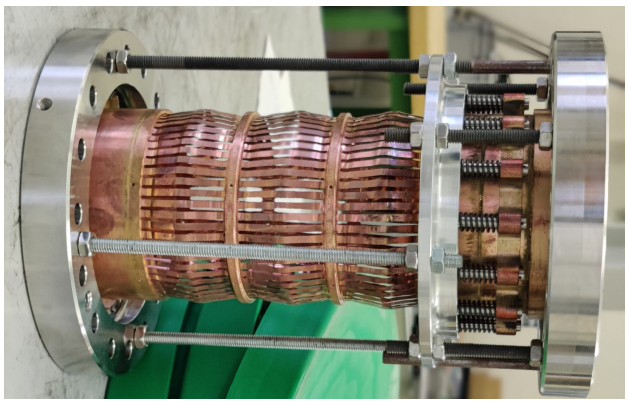

Figure 1: Picture of the deformable RF contact brigde (DRF) with three convolutions and pre-loaded springs.

diameter ⌀ 63 mm, ⌀ 150 mm and ⌀ 250 mm, depending on the individual placement in the accelerator. For this new bridge concept, extensive mechanical and material analysis and tests were conducted, and the mechanical limits and anticipated lifetime were established [2].

We have started the prototyping process and are approaching the beginning of the series production. Consequently, the impedance must be carefully assessed prior to installation as the general parameters of the final HL-LHC vacuum design have been defined. This step ensures that the system operates at optimal performance levels and meets all required specifications.

CST 3D MODEL

Based on mechanical drawings for the prototyping, a simplified DRF model has been reconstructed in CST Suite simulation code for this investigation, as seen in the animated Fig. 2. The convolution height and length are independent of the diameter. The DRF contact bridge consists of copper-beryllium (CuBe) C17410 with a room-temperature conductivity of $\kappa_{\mathrm{CuBe}} = 10.3\,\mathrm{MS/m}$. Symmetrically on the extremeties of the DRF, 40 mm long round stainless steel 316 beam pipes with $\kappa_{\mathrm{SS316}} = 1.3\,\mathrm{MS/m}$ are added in the simulation. The surrounding cylinder of stainless steel 316 represents the bellow with the designed diameters.

The preloaded springs, as shown in Fig. 1, retain the DRF convolution in a particular stretched position with a consequential nominal convolution angle of $\alpha_{\mathrm{nomi}} = 11°$, which refers to the free state of the surrounding bellows. On the other hand, a maximum 20 mm axial compression is expected as the worst-case scenario, translating to a convolution angle of $\alpha_{\mathrm{wcase}} \approx 43°$. Consequently, the study focuses on these two convolution angles.

* patrick.krkotic@cern.ch
† sergio.calatroni@cern.ch

ISBN: 978-3-95450-231-8 ISSN: 2673-5490 doi: 10.18429/JACoW-IPAC2023-WEPL153

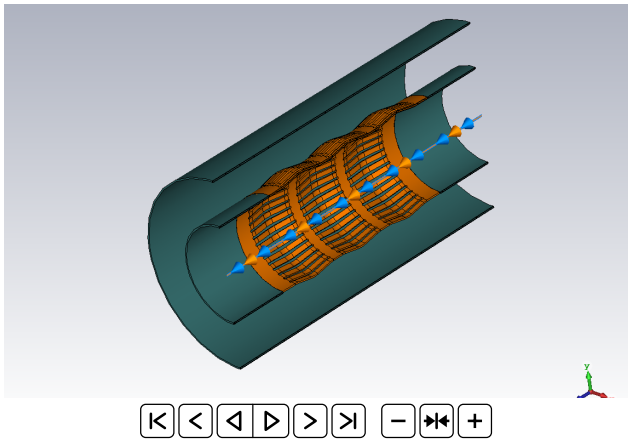

Figure 2: Longitudinal cross-section of the DRF ⌀ 63 mm with simplified bellow structure.

DRF IMPEDANCE ASSESSMENT

CST Particle Studio was used to perform simulations in the time domain, and CST MW Studios for the frequency domain [3]. As the primary interest of investigation lies within the longitudinal and transverse impedance, open boundary conditions at both ends of the beam pipe were used following the approach described in [4]. The particle beam parameters are is based on the values given in the HL-LHC report [5]. The total bunch charge equals $C = 2.2 \cdot 10^{11} e$, where e refers to the elementary charge. The RMS bunch length (full-width at half maximum equivalent Gaussian) is $\sigma_z = 90$ mm and it corresponds to a maximum frequency domain simulation limit of ≈ 2.7 GHz. The beam is considered to be relativistic with $\beta = 1$.

Simulations in Time Domain

The DRF is an axisymmetric accelerator element; thus, the longitudinal impedance can be evaluated by maintaining both source and test beam paths in CST at their nominal positions in the centre of the device under test. Figure 3 shows the longitudinal impedance extracted from CST for $\alpha_{\text{wcase}} = 43°$ as a function of frequency for all three DRF structures. As can be seen, conversely to the DRF ⌀ 63 mm, the DRF ⌀ 150 mm and DRF ⌀ 250 mm show resonances at $f_0 \approx 1$ GHz and $f_0 \approx 1.5$ GHz, respectively; thus, within the beam spectrum. The reason lies within the difference in cut-off frequencies summarised in Table 1. It shall be mentioned, that the results shown in Fig. 3 result from simulations performed with short wakelenghts in order to identify resonances; thus the peaks are not representative for the quality factor, which is estimated with the eigenmode solver, as explained in the next section.

The longitudinal impedance estimated in CST is fitted with a linear polynomial function $Z_{||}^{\text{CST}}(f) = m \cdot f$ at low frequencies to determine the longitudinal broadband impedance. The impedance value is estimated over [6]:

$$\left(\frac{Z}{n}\right)_{||} = m \cdot f_{\text{rev}}, \qquad (1)$$

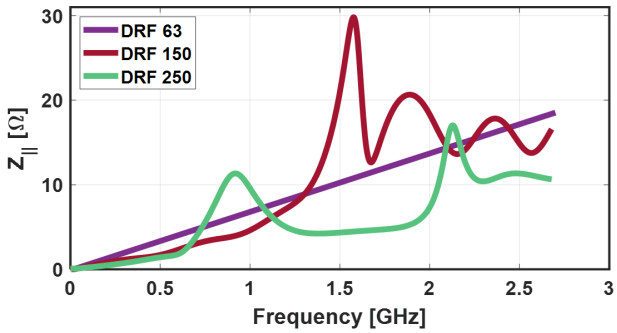

Figure 3: Longitudinal impedance given by the CST wakefield solver for the three different DRF diameters simulated with short wakelengths in order to identify existing resonances.

where $n = f_{\text{rev}}/f$ and $f_{\text{rev}} = 11245$ Hz is the revolution frequency of the HL-LHC. The benefit of determining the $\left(\frac{Z}{n}\right)_{||}$ value lies in the possibility of summing the value of each device and giving an expected impedance budget for all DRF modules to be installed in one accelerator.

The results obtained evaluating the imaginary part of the longitudinal impedance for the nominal and worst-case convolution angle are summarised in Fig. 4. Two main features are observed: the impedance decreases with the diameter of the DRF, whereas it increases with the convolution angle. In order to facilitate the process for the systematic study of angle, diameter, longitudinal and transverse impedances, a Python-Induced CST Solver Automation (PICSA) was developed. With this automation of the simulation process, a convergence study was performed for each diameter in order to find a reasonable amount of mesh cells necessary so that the results do not vary more than 2%. Hence, the studies were performed with 40, 130, and 250 million mesh cells for the ⌀63 mm, ⌀150 mm and ⌀250 mm, respectively. Additionally, a parametric study of the convolution angle α for the DRF ⌀ 63 mm revealed a linear impedance behaviour between $\alpha \approx 10°$ to $\alpha \approx 50°$. The findings suggest that between the two angles of interest α_{nom} and α_{wcase}, a linear increase in impedance is given.

It is usually sufficient to evaluate the beam dynamics to only the first order, which involves only slight transverse

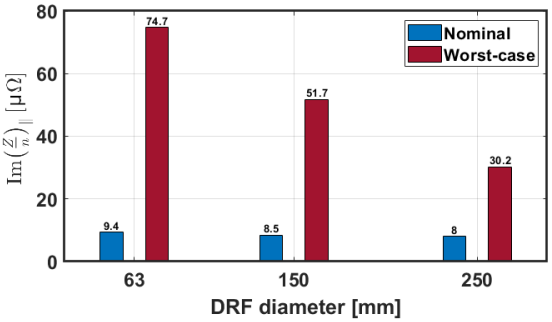

Figure 4: Imaginary part of the longitudinal impedance for the DRF and different diameters.

ISBN: 978-3-95450-231-8 ISSN: 2673-5490 doi: 10.18429/JACoW-IPAC2023-WEPL153

disturbances [6]. Second and higher-order terms can be regarded as insignificant, assuming there is no coupling between the horizontal and vertical planes and the transverse displacements are sufficiently small [6]. This entails separating the impedance into horizontal and vertical components as well as the dipolar (or driving impedance) and quadrupolar (or detuning impedance), which are solely dependent on the displacement s of the source or test path in the simulation [7] $Z_\perp \approx Z_{\perp,0} + s \cdot Z_{\perp,\mathrm{dip}} + s \cdot Z_{\perp,\mathrm{quad}}$ In the above notation, the transverse impedance has two components: $Z_{\perp,0}$ which is unaffected by the offsets of the particles, and $Z_{\perp,\mathrm{dip,quad}}$, which is linearly proportional to the offset of the source/test particle, respectively. The perturbed pathways must be sufficiently close to the nominal ones to keep the linear approximation, whereas the simulation domain needs to be appropriately tuned to guarantee that the two pathways have an adequate resolution. Thus, it is crucial to remember that determining the transverse impedance with a too-small displacement might be numerically challenging [6]. In the average beta can be used for the beam dynamics simulations; therefore, the CST dipolar/quadrupolar impedance data is post-processed over:

$$Z_{\perp_{\mathrm{op}}} = \frac{Z_{\perp,\mathrm{driv,detu}} - Z_{\perp,0}}{s \cdot \beta_{\mathrm{avg}}} \cdot \beta_{\mathrm{pos}}, \qquad (2)$$

where β_{pos} and β_{avg} refer to the beta function at the position of the specific device and the average beta function of the machine, respectively. In the LHC, the average beta values are around $\beta_{\mathrm{avg}}^{\mathrm{horiz}} = 68\,\mathrm{m}$ horizontally and $\beta_{\mathrm{avg}}^{\mathrm{vert}} = 70\,\mathrm{m}$ vertically [8].

Besides a displacement study in one plane, three scenarios were simulated to determine if there is an effect of the asymmetric azimuthal RF fingers distribution in the DRF. As an axisymmetric device, the horizontal and vertical components should not differ. The findings of this study indicated minor fluctuations in the impedance values based on the positioning of the beam and integration path without showing a pattern in the results. Eventually, the variations in these values, which are about 3%, most probably originated from the emerging numerical inaccuracies rather than the influence of the asymmetry itself. This can be interpreted as the uncertainty of the results shown in Fig. 5. The imaginary transverse impedances are normalised to the HL-LHC's average beta function. Similarly to the longitudinal impedance, the values decrease as a function of diameter and increase as a function of convolution angle. Moreover, the dipolar component is larger than the quadrupolar component.

Simulations in Frequency Domain

Based on the wakefield solver's time domain capabilities and the fast-Fourier transformation used as post-processing to determine impedance, CST would need a vanishing wakefield to conduct the FFT sensibly; hence, a very long wakelength in the simulations [6]. This emphasises the difficulty of extrapolating common frequency domain characteristics from time domain codes, such as the shunt impedance R_S and unloaded quality factor Q_0 of resonances.

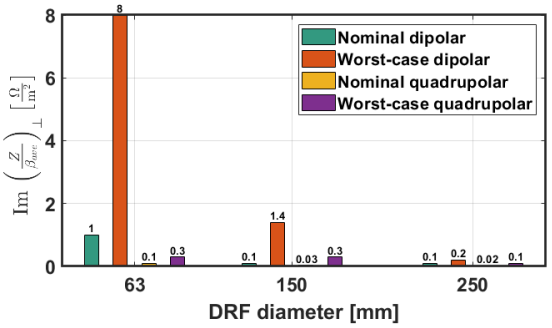

Figure 5: Longitudinal cross-section of the DRF ⌀ 63 mm with simplified bellow structure.

It should be noted that the eigenmode solver, unlike the Wakefield solver, requires the structure to be closed, which causes parasitic trapped modes to develop that depend on the device's specified volume. Owing to this, we simulated the DRF in various scenarios by extending the simulation domain with attached beam pipes of various lengths to find (if existing) resonant trapped modes of the DRF. The results have shown that the shunt impedance R_S decreases as a function of the attached beam pipe length for all DRF at the convolution angle of $\alpha_{\mathrm{nomi}} = 11°$. The decreasing behaviour indicates that the mode is not trapped at the given angle but propagates through the resistive beam pipe. Conversely, by looking at the worst-case scenario, a steady behaviour of the shunt impedance is found. These findings suggest that these modes are trapped in the DRF structure due to the higher angle. The values for this case are summarised in Table 1.

Table 1: Characteristic resonance parameters for the different DRF modules at $\alpha_{\mathrm{wcase}} = 43°$.

	63	**150**	**250**
$f_{\mathrm{cut-off}}$ [GHz]	2.7	1.2	0.7
f_0 [GHz]	3.3	1.5	0.9
Q_0 10^4	1.0	0.9	0.9
R_S [kΩ]	1.5	2.8	0.5

CONCLUSION

In this study, we explored the electromagnetic behaviour of deformable RF contact bridges to be used in the HL-LHC upgrade. We found the characteristic nominal and worst-case scenario impedance contributions. The findings suggest that in the worst-case scenario large diameter bellows are of concern as they would lead to large power loss, e.g. 500 Ohm at 0.9 GHz. However, further studies should adapt to the final module and investigate the collective effects as well as dissipated power with a refined model to understand better stress and temperatures distributions for vacuum stability.

ACKNOWLEDGEMENTS

The Authors would like to express their gratitude towards Leonardo Sito and Nicolas Mounet for their support on this numerical study, fruitful discussions and valuable input.

ISBN: 978-3-95450-231-8 ISSN: 2673-5490 doi: 10.18429/JACoW-IPAC2023-WEPL153

REFERENCES

[1] C. Garion, A. Lacroix, and H. Rambeau, "Development of a New RF Finger Concept for Vacuum Beam Line Interconnections," in *Proc. IPAC'12*, (New Orleans, LA, USA, May 2012), JACoW Publishing, Geneva, Switzerland, pp. 2531–2533.

[2] J. P. Espinos and C. Garion, "Analysis and Testing of a New RF Bridge Concept as an Alternative to Conventional Sliding RF Fingers in LHC," in *Proc. IPAC'16*, (Busan, Korea, May 2016), JACoW Publishing, Geneva, Switzerland, pp. 3660–3662. DOI: 10.18429/JACoW-IPAC2016-THPMY006.

[3] "Cst studio suite." Dassault Systemes. (2022).

[4] O. Kononenko, F. Caspers, A. Grudiev, E. Métral, and B. Salvant, "Impedance Studies for VMTSA Module of LHC Equipped with RF Fingers," in *Proc. IPAC'13*, (Shanghai, China, May 2013), JACoW Publishing, Geneva, Switzerland, pp. 1805–1807.

[5] O. Brüning and et al., *High-Luminosity Large Hadron Collider (HL-LHC): Technical design report* (CERN Yellow Reports: Monographs). Geneva: CERN, 2020.

[6] C. Zannini, "Electromagnetic Simulation of CERN accelerator Components and Experimental Applications," 2013.

[7] V. Vlachodimitropoulos, M. J. Barnes, A. Chmielinska, and L. Ducimetière, "Transverse Impedance Measurements and Simulations of the LHC Injection Kicker Magnet," in *Proc. IPAC'19*, (Melbourne, Australia, May 2019), JACoW Publishing, Geneva, Switzerland, pp. 3986–3989.

[8] N. Mounet, *Private Communication*, 2023.